ARTICLE

Simulating Mechanical Deformation in Nanomaterials with Application for Energy Storage in Nanoporous Architectures

Thi X. T. Sayle,[†] Phuti E. Ngoepe,[‡] and Dean C. Sayle[†,*]

[†]DASSR, Cranfield University, Defence Academy of the United Kingdom, Shrivenham SN6 8LA, United Kingdom, and [‡]Materials Modeling Centre, School of Physical and Mineral Sciences, University of Limpopo, Private Bag x1106, Sovenga 0727, South Africa

ABSTRACT Central to porous nanomaterials, with applications spanning catalysts to fuel cells is their (perceived) "fragile" structure, which must remain structurally intact during application lifespan. Here, we use atomistic simulation to explore the mechanical strength of a porous nanomaterial as a first step to characterizing the structural durability of nanoporous materials. In particular, we simulate the mechanical deformation of mesoporous Li—MnO_2 under stress using molecular dynamics simulation. Specifically, such rechargeable Li-ion battery materials suffer volume changes during charge/discharge cycles as Li ions are repeatedly inserted and extracted from the host β-MnO_2 causing failure as a result of localized stress. However, mesoporous β-MnO_2 does not suffer structural collapse during cycling. To explain this behavior, we generate a full atomistic model of mesoporous β-MnO_2 and simulate localized stress associated with charge/discharge cycles. We calculate that mesoporous β-MnO_2 undergoes a volume expansion of about 16% when Li is fully intercalated, which can only be sustained without structural collapse, if the nanoarchitecture is symmetrically porous, enabling elastic deformation during intercalation. Conversely, we predict that unsymmetric materials, such as nanoparticulate β-MnO_2, deform plastically, resulting in structural collapse of (Li) storage sites and blocked transport pathways; animations revealing elastic and plastic deformation mechanisms under mechanical load and crystallization of mesoporous Li—MnO_2 are presented at the atomistic level.

KEYWORDS: rechargeable · Li-ion battery · nanomechanics · manganese oxide · crystallization · mechanism · mesoporous

Central to the exploitation of nanoporous materials in applications such as catalysis, photocatalysis, sensor, foams, MEMS, fuel cell, battery, solar cell, is their (perceived) "fragile" structure, which must nevertheless resist structural damage during application lifespan. However, little is know about the factors that improve or are deleterious to the mechanical durability of nanoporous materials. Mechanical testing of nanostructures is challenging because of the difficulties in synthesizing prescribed architectures with controllable and well-characterized microstructural imperfections. Moreover, complex *in situ* mechanical testing experiments need to be performed. Clearly, the ability to calculate mechanical properties and simulate deformation mechanisms for nanoporous materials at the atomistic level, will provide considerable insight for experiment, analogous to the wealth of simulation data that have already been amassed for bulk materials. Here, we demonstrate how the mechanical properties of a crystalline nanoporous material with prescribed architecture and characterized microstructure can be calculated by simulating uniaxial and hydrostatic compressive and tensile strain using molecular dynamics simulation. To explore the viability of using simulation to predict mechanically robust architectures, we simulate nanoporous Li—MnO_2 as a model system. Specifically, such rechargeable Li-ion battery materials suffer volume changes during charge/discharge cycles as Li ions are repeatedly inserted and extracted from the host β-MnO_2 causing failure as a result of localized stress. However, mesoporous β-MnO_2 does not suffer structural collapse during cycling. To explain this behavior we generate a full atomistic model of mesoporous β-MnO_2 and simulate localized stress associated with charge/discharge cycles using molecular dynamics simulation. We calculate that mesoporous β-MnO_2 undergoes a volume expansion of about 16% when Li is fully intercalated, which can only be sustained without structural collapse, if the nanoarchitecture is symmetrically porous, enabling elastic deformation during intercalation. Conversely, we predict that unsymmetric materials, such as nanoparticulate β-MnO_2 or especially the bulk parent material deform plastically, resulting in structural collapse of (Li) storage sites and blocked transport pathways; animations revealing elastic and plastic deformation mechanisms under

*Address correspondence to d.c.sayle@cranfield.ac.uk.

Received for review August 7, 2009 and accepted September 14, 2009.

Published online September 23, 2009. 10.1021/nn9009592 CCC: $40.75

mechanical load and crystallization of mesoporous Li−MnO_2 are presented at the atomistic level.

Nanoporous materials are more than just the nm extension in scale of macromaterials. Unique morphologies and properties can be generated with no analogue in the macroworld. For example, porous metal oxides promise size and shape selective catalysis as epitomised by zeolites,[1] but offer potentially far greater choice of metal cations, cavity shape, size, porosity and connectivity. Moreover, the internal surfaces, curvature (convex and concave) and hence chemical reactivities differ from the parent bulk material. Accordingly, it is not surprising that considerable efforts have been directed at the synthesis,[2] characterization,[3] and remarkable properties of nanoporous materials with applications spanning catalysis,[4] rechargeable batteries,[5] photocatalysis,[6] gas sensors[7] and even microbial fuel cells.[8]

Fabrication of mechanically robust nanoporous materials requires an understanding of (structural) features that prove detrimental or improve their mechanical resilience. Such knowledge would likely be acquired by systematically synthesizing nanoporous architectures and then measuring their mechanical properties to yield architecture-property correlations: To this end, "bottom-up" synthetic strategies, using nanobuilding blocks, enables one to fabricate potentially any architecture. However, because of their small size the nanobuilding blocks need to be "self-assembled",[9] and therefore prescribing particular architectures is difficult. Nevertheless, a degree of control over the positioning of the nanobuilding blocks can be achieved using, for example, surfactants,[10] prefabricated templates,[11] and even DNA.[12] In addition to the architectural shape, microstructural imperfections will also play a pivotal role. Specifically, it is well-known that dislocations, grainboundaries, and (point) defects govern the mechanical properties of a material.[13] Accordingly, methods for prescribing and characterizing particular microstructures are needed.[14] The mechanical properties can then be measured, albeit the challenges are again considerable requiring *in situ* mechanical deformation testing.[15−17]

Atomistic simulation offers a complementary technique to explore the mechanical properties of a nanoporous material as a function of structure, analogous to the wealth of insights derived from simulating fully dense nanomaterials.[18] In particular, model nanobuilding blocks can easily be positioned at *any* location to formulate atomistic models of nanoporous materials with prescribed architectures.[19] Microstructural imperfections can be introduced into the structural model and characterized using molecular graphics. The mechanical properties can then be calculated with standard approaches using the structural model.[20,21]

Here, we perform such a study using mesoporous β-MnO_2, which is potentially an important component material in rechargeable Li-ion batteries[22,5] with applications spanning electric vehicles to smart grid. In particular, the thin walls of the mesoporous MnO_2 facilitate a "significant increase in the rate of lithium insertion/removal, because of the short distances needed for lithium-ion transport together with high surface areas, which permit high contact areas with the electrolyte and hence a high lithium-ion flux across the interface".[23]

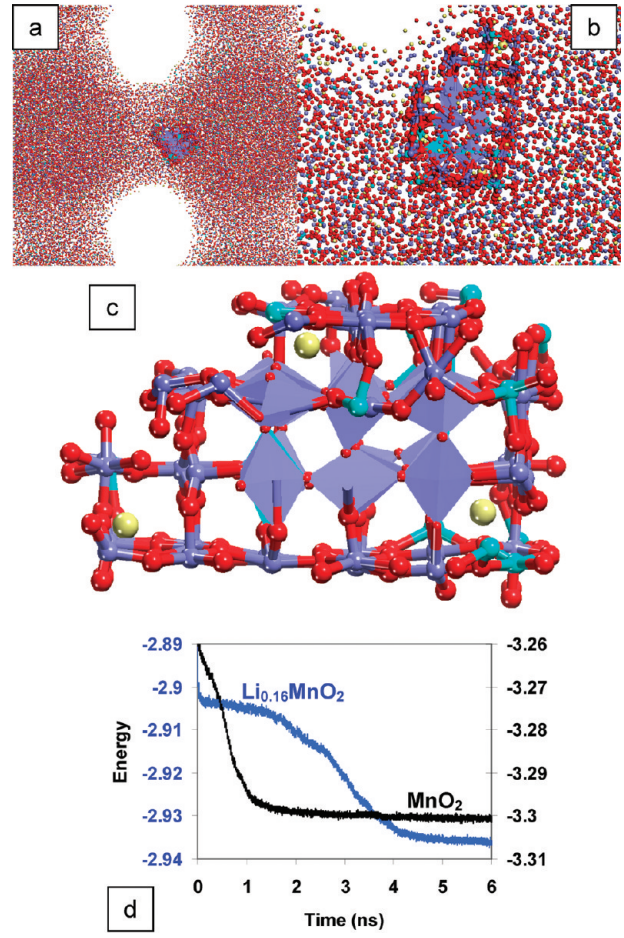

Figure 1. Atomistic structure of the nucleating seed, which evolves spontaneously within the $Li_{0.16}MnO_2$ system facilitating its crystallization: (a) seed encapsulated within the amorphous sea of ions; (b) enlarged region of panel a; (c) structure of the seed. Li is colored yellow, Mn^{4+} is blue, Mn^{3+} is light blue, and O is red; (d) configurational energy, calculated as a function of time during the crystallization. Energy is given in 100000 eV.

Symmetrically porous β-MnO_2 can host the storage and transport of Li (charge carriers) up to a composition of $Li_{0.92}MnO_2$, commensurate with 284 $mAhg^{-1}$, yet retain its structural integrity despite the high lattice expansion and contraction associated with charge/discharge cycles. Conversely, the nanoparticulate and especially the bulk parent material are unsuitable. To understand why the mesoporous architecture conveys such exemplary electrochemical properties, we construct a model and simulate mechanical load.

To calculate accurately the mechanical properties of the material, the model must capture all hierarchical levels of structural complexity that will influence its nanomechanical properties. These include (a) the framework architecture and topographical shape, (b)

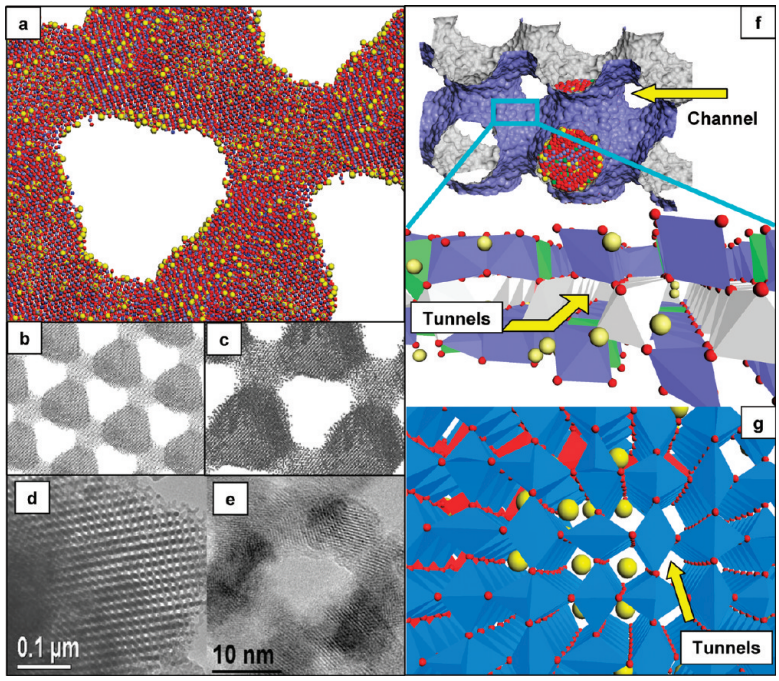

Figure 2. Atomistic models for mesoporous $Li_{0.16}MnO_2$: (a) slice cut through the atomistic model revealing Li ions, which locate within the host β-MnO_2 and decorate the (internal) surfaces of the β-MnO_2; (b) atomistic model revealing the symmetrically porous architecture; (c) enlarged region of panel b; (d, e) HRTEM of $Li_{0.92}MnO_2$ (to compare with atomistic models) (Reproduced with permission from ref 5. Copyright 2007 Wiley-VCH Verlag GmbH & Co. KGaA.) (f) Surface rendered model of the porous architecture revealing 1 × 1 tunnels exposed and open at the surface, which enable Li^+ ions to insert into the mesoporous β-MnO_2 framework; (g) perspective view looking along the 1 × 1 tunnels, some of which are occupied by Li^+; MnO_6 are shown as polyhedra. The images are not schematic; rather they represent atom positions corresponding to the atomistic model. Li is colored yellow, oxygen is red, and manganese is blue.

microstructural features including dislocations/grain-boundaries and defects, and (c) the polymorphic crystal structure. Crucially, the relationship between these hierarchical levels of structural complexity—such as the orientation of the crystal structure with respect to the framework architecture, position of grain-boundaries—may prove pivotal. Experimentally, the architecture, microstructure, and crystal structures evolve synergistically during crystallization.[24] Accordingly, we propose that the best and arguably easiest way to realize a realistic structural model is to simulate the (synthetic) processes that led to its fabrication—specifically to simulate crystallization.[25]

RESULTS

In this section we describe the simulated crystallization of $Li_{0.16}MnO_2$, microstructural features that evolved within the model as a consequence of simulating the crystallization and finally the mechanical properties calculated using the model.

Crystallization. Analysis of the simulated crystallization, using molecular graphics, revealed the spontaneous evolution of a pseudocrystalline seed, conforming to the β-MnO_2 polymorph, Figure 1, in accord with experiment, which nucleated the crystallization of the surrounding amorphous sea of ions. We note that the host MnO_2 was able to crystallize around the Li species enabling the Li to be located within the 1 × 1 tunnels of the β-MnO_2 as observed experimentally.[22] Inspection of the crystalline seed, Figure 1a−c reveals three Li species within the host MnO_2 and associated with neighboring Mn^{3+} species.

Configurational energies, calculated for $Li_{0.16}MnO_2$ and β-MnO_2 during this process, are shown in Figure 1d. The energy difference between the starting (amorphous) and final (crystalline) states reflects loosely the heat of crystallization; animations revealing the crystallization (mechanism) at the atomistic level are available as Supporting Information. The density and surface area calculated for $Li_{0.16}MnO_2$ are 2.8 g/cm^3 and 168m^2/g, respectively, with a 4−8 nm wall thickness in accord with experiment.[22] We predict that during Li intercalation, associated with charge/discharge cycles, the host lattice contracts/expands by 16%, respectively. In particular, when Li is introduced into the β-MnO_2 host (discharging), the volume increases (per MnO_2 unit) from 28.4 Å^3 (pure β-MnO_2) to 29.2 ($Li_{0.16}MnO_2$), a 2.8% increase. Extrapolated to the maximum intercalation levels of Li achieved experimentally, $Li_{0.92}MnO_2$[5] yields a 16% volume increase. Specifically, the observed limit of 0.92 Li per MnO_2 unit is 5.75 times higher than our model, which comprises 0.16 Li per MnO_2 unit. If we assume that the lattice expands linearly with the introduction of Li, then the expansion associated with Li intercalation into β-MnO_2 up to $Li_{0.92}MnO_2$ is predicted to be about 16%.

Inspection of the final, low temperature structural model, using graphical techniques reveals that the simulated crystallization has facilitated the evolution of a variety of important microstructural features observed experimentally,[26] including grain-boundaries, twin-boundaries, microtwinning, and point defects, which are described in the following section.

Microstructural Features. The final low temperature structure for the $Li_{0.16}MnO_2$ model, compared with experiment, is shown in Figure 2, and reveals Li ions located within the framework walls of the β-MnO_2 and also decorating its internal surfaces, Figure 2a. An enlargement of a particular region of the β-MnO_2 surface, Figure 2f, reveals 1 × 1 tunnels, which terminate at the internal surfaces and remain "open" enabling Li (charge carriers) to insert into the host; Figure 2g reveals several Li species that reside within the 1 × 1 tunnels of the host.

A slice cut through the β-MnO_2, Figure 3a, reveals complex (predominantly twin) grain-boundary structures with curved, rather than planar, interfacial planes. The individual grains exhibit low angle rotations with respect to one another, which further obscures identification of the boundaries. We attribute such mis-

orientation to the convex and concave architecture of the framework. A slice cut through the $Li_{0.16}MnO_2$ framework, with polyhedral rendering of the individual MnO_6 octahedra to aid visualization of the 1 × 1 tunnels, Figure 3b,c shows the distribution of Mn^{3+} species within the lattice together with Li species located within the tunnels. A twin boundary is shown more clearly in Figure 3d. In Figure 3e a region conforming to ramsdellite (2 × 2 tunnel structure) is visible (oval).

Experimentally, ramsdellite intergrowths have been observed within pyrolusite (γ-MnO_2).[26] Specifically, it was proposed that the ramsdellite domains are stabilized with protons (Ruetschi defects). In previous simulations of β-MnO_2, we found no evidence of ramsdellite intergrowths using simulated amorphization and crystallization. We propose therefore that its appearance in our model for Li−MnO_2 suggests that the Li species, which are located within the 1 × 1 tunnels, act as a "scaffold" stabilizing the 2 × 2 tunnel, similar to the proposal that protons stabilize ramsdellite intergrowths. Specifically, the 2 × 2 channel appears to be stabilized by two neighboring Li species, which are bound to the host MnO_2 lattice *via* Mn^{3+} species (colored red). Balachandran and co-workers proposed[27] that "Mn vacancies compensated by protons (Ruetschi defects), ubiquitously present in commercial MnO_2, are shown to have a dramatic effect on phase stability. The stabilizing effects of Ruetschi defects may explain the presence in MnO_2 of ramsdellite and twinning, both of which are unstable in the pure material." Closer inspection of the ramsdellite intergrowth, Figure 4e, reveals the presence of a Mn vacancy (highlighted by the arrow). Similar to the twin-boundaries, the evolution of vacancies within the structural model is achieved during the crystallization process.

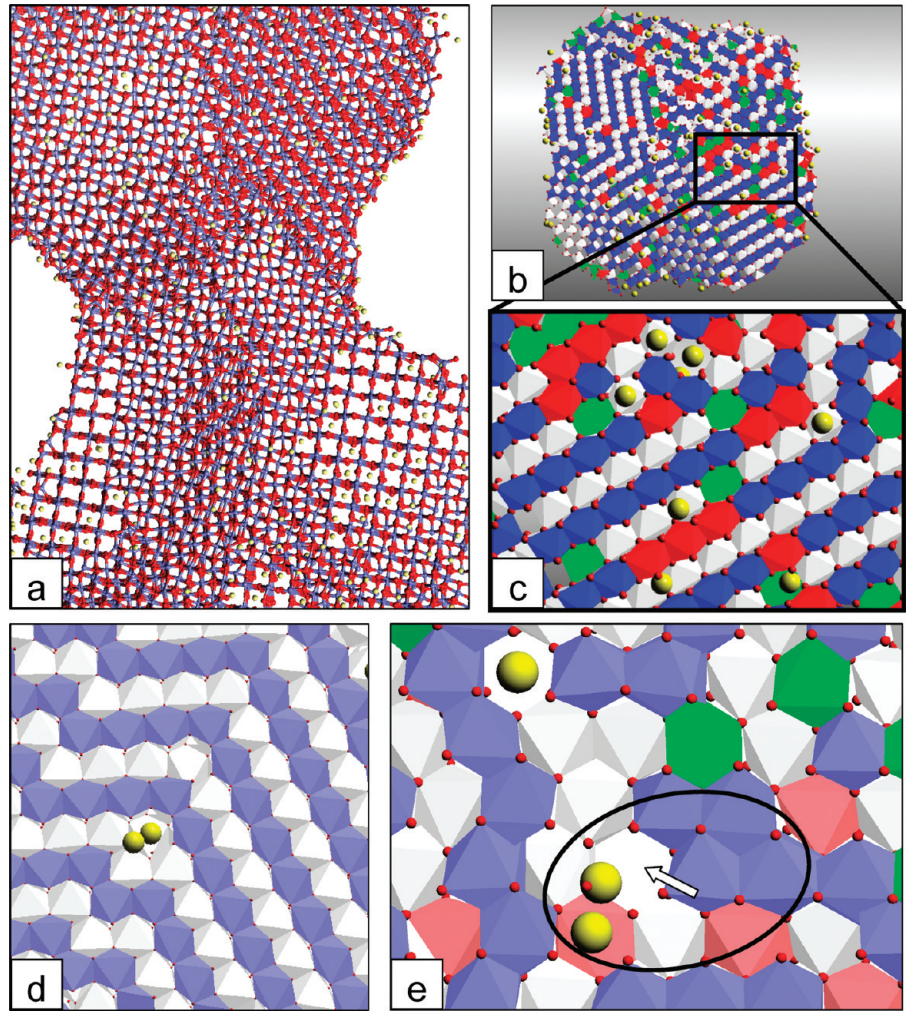

Figure 3. Microstructural features. (a) Slice cut through the mesoporous $Li_{0.16}MnO_2$ revealing the complex grain-boundary structure. (b) Polyhedral representation of the MnO_6 octahedra revealing the 1 × 1 tunnels and the Li ions that locate within the tunnels; (c) enlarged segment of panel b; (d) region depicting a twin-boundary; (e) region comprising a 2 × 2 tunnel (oval) indicative of a ramsdellite intergrowth; the arrow shows the position of a Mn vacancy. Li is colored yellow, Mn^{4+} are colored blue (upper plane) and white (lower plane); Mn^{3+} are green (upper plane) and red (lower plane). Mn^{3+} species in panels a and d are not distinguished from Mn^{4+}.

Mechanical Properties. Stress−strain curves, calculated for $Li_{0.16}MnO_2$, Figure 4, and β-MnO_2 (not shown), reveal that the material expands elastically up to 5% (uniaxial) and 10% (hydrostatic) strain with plastic deformation occurring above these levels. Animations, revealing elastic and plastic deformation mechanisms at the atomistic level in both β-MnO_2 and $Li_{0.16}MnO_2$, are available as Supporting Information.

The structure of mesoporous $Li_{0.16}MnO_2$ after uniaxial tension is shown in Figure 4c and reveals that the material fractures along its thinnest wall (pillar); the unstrained starting structure is shown in Figure 4d. Conversely, Figure 4e shows the structure after hydrostatic compression. Analysis of this structure and animations of the compression induced deformation reveal plastic deformation and failure occur *via* grain-boundary sliding culminating in the amorphization of grain-boundary regions. Crucially, the 1 × 1 tunnels, which facilitate Li storage and transport, are lost, and Li ions become trapped within amorphous MnO_2, Figure 4f.

DISCUSSION

When used as an electrode in a rechargeable Li-ion battery, symmetrically porous β-MnO_2 can host flooding of all pores by electrolyte because of pore accessibility. Accordingly, during charge/discharge cycles, Li

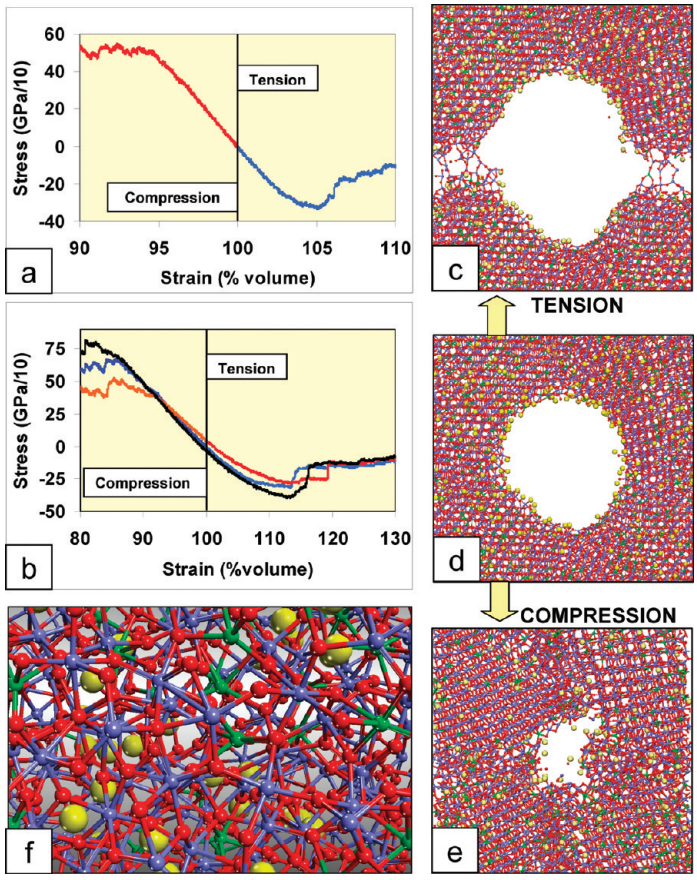

Figure 4. Mesoporous $Li_{0.16}MnO_2$ under tensile and compressive strain. Stress−strain curve for (a) uniaxial strain; (b) hydrostatic strain. Each trace corresponds to the strain along deformation axes. A volume of 100 indicates the unstrained material. Atomistic structure of the $Li_{0.16}MnO_6$ mesostructure after (c) uniaxial tension (volume = 117%); (d) starting (unstrained) structure; (e) hydrostatic compression (volume = 63%); (f) enlarged segment of panel e showing Li ions trapped within an amorphous region of the MnO_2 host.

can insert at all positions on the internal surfaces enabling the entire symmetrically porous β-MnO_2 architecture to expand homogeneously; any slight inhomogeneity in either the structure or insertion process can be accommodated by elastic deformation (up to 10% volume change). Accordingly, the symmetrically porous β-MnO_2 can expand and contract elastically during charge/discharge cycles with no structural degradation. Conversely, for nonsymmetrically porous architectures, such as nanoparticulate β-MnO_2, or especially the bulk parent material, particular domains will not be accessible to the electrolyte. Accordingly, Li transport must proceed by entering the host lattice at sites accessible to the electrolyte and then move along the 1 × 1 tunnels, within the framework of the host lattice, to reach "inaccessible" domains. As the Li enters accessible regions, the β-MnO_2 host can expand by up to 16% (theoretical maximum for $Li_{0.92}MnO_2$ observed experimentally) compared to inaccessible regions. At such levels of strain, our simulations reveal that plastic deformation will occur, destroying the 1D channels and connectivity pathways thus rendering the β-MnO_2 useless as an intercalation host.

CONCLUSION

Nanoporous materials offer unique chemical, physical, and mechanical properties compared to their bulk counterparts. However, a major limitation to their application in a wide variety of applications is their perceived fragility. To determine features that contribute to improved mechanical durability necessitates a systematic enumeration of the mechanical properties as a function of architecture and (micro)structure. Such an endeavor is challenging experimentally because one cannot simply fabricate nanostructures with prescribed architectures from nanobuilding blocks and then measure their mechanical properties analogous to methods used at the macroscale, rather, innovative methods of (self) assembly into desired architectures need to be developed and then challenging *in situ* mechanical testing performed; control and characterization of microstructure further adds to the complexity and hence difficulty associated with such experiments. On the other hand, atomistic computer simulation is well positioned to undertake such an enumeration. Specifically, we have shown how amorphous model nanobuilding blocks, playing the role of atoms in this metacrystallography, can be easily positioned into any location to attain desired (prescribed) architectures. The nanoparticles can then be encouraged to agglomerate, under MD simulation, to formulate the walls of the nanoporous framework architecture. To calculate the mechanical properties with sufficient accuracy such that the results are of value to experiment requires that the model captures three levels of hierarchical structural complexity: the architectural shape and morphology, such as convex and concave architectures, microstructural features including grain-boundaries, microtwinning, and point defects, together with the polymorphic crystal structure. Introducing such structural complexity, including their synergy of interaction, can be achieved by simulating crystallization and microstructural characterization performed using molecular graphics.

The methodology was tested using nanoporous MnO_2—an industrially important material with respect to rechargeable Li ion batteries. Our simulations on Li−MnO_2 reveal that at high strain, the mesoporous material deformed plastically; failure mechanisms under compression-induced plasticity are associated with slip along grain-boundary regions, which indicates that the microstructure plays a pivotal role in the mechanical properties.

Our simulations reveal that for MnO_2 to be a viable host within rechargeable battery systems, the material must be symmetrically porous to enable the material to expand linearly with Li intercalation. Nonsymmetrically porous MnO_2 will suffer plastic deformation. We propose that other (mesoporous) intercalation hosts will follow similar mechanisms.

METHOD

In this section we describe the potential models used to represent the interactions between component ions together with the code used to perform the MD simulations and the strategy for generating prescribed atomistic models for nanoporous materials and then simulating their mechanical properties.

Potential Models. All calculations, presented in this study, are based upon the Born model of the ionic solid, in which a charge is assigned to each atom and the long-range attractive interactions between these charged ions is balanced by short-range repulsive (electron−electron) interactions. Model parameters, used to describe Li−MnO_2 are given in Table 1. These parameters have been used previously to model the structure of nanoparticles, nanorods, nanosheets, and nanoporous architectures of MnO_2.[28,29]

Simulation Code. The DL_POLY code was used to perform all the molecular dynamics (MD) simulations.[30] All simulations were performed using three-dimensional periodic boundary conditions, and therefore the model framework structures represent periodic systems, which are infinitely repeating. Molecular graphics was performed using Visual Molecular Dynamics (VMD)[31] and Materials Studio.

Strategy to Generate Nanoporous Architectures. To generate the atomistic model, amorphous nanoparticles of Li_xMnO_2 were positioned into a simulation cell to accord closely with the real material. In particular, model nanobuilding blocks, playing the role of atoms in this meta-crystallography, can easily be positioned into any location to attain desired architectures.[19] Neighboring nanoparticles were then allowed to agglomerate to formulate the walls of the porous architecture, and the system crystallized. We note that simulated crystallization of Li−MnO_2 proved very difficult. In particular, systems with high concentrations of Li remained amorphous even after running MD simulation for time scales in excess of 10000 ps. This was attributed to the fast moving Li species perturbing the evolution of a viable seed needed to nucleate crystallization. Accordingly, the Li concentration was reduced sequentially in an attempt to induce crystallization. Specifically, crystallization of the Li_xMnO_2 system was successful up to intercalation levels commensurate with $Li_{0.16}MnO_2$. Finally, the structural response to tensile and compressive strain were simulated. The process is illustrated in Figure 5; the nanoarchitecture comprises mesoporous MnO_2 with channels traversing all three spatial dimensions.

Generating an atomistic model for $Li_{0.16}MnO_2$ was achieved by cutting a cube of stoichiometric β-MnO_2, comprising 24696 atoms, from the parent bulk material. There were 1236 Li^+ ions introduced by substituting randomly equal numbers of Mn^{4+} and O^2 atoms with Li^+; 1236 Mn^{4+} species were then reduced to Mn^{3+}, and 618 oxygen atoms were removed to facilitate charge neutrality. Similar to the introduction of Li^+ species, the Mn^{3+} and O vacancies were chosen at random. The rationale underlying the random selection of ions is that within the amorphous phase, all the ions have high mobilities and therefore can move, under MD, to energetically favorable positions during crystallization. Tension induced amorphization[28] was used to generate an amorphous nanoparticle and was achieved by expanding the lattice by 36% and applying MD simulation at 2000 K for 750 ps. The cell dimensions were then adjusted to enable neighboring nanoparticles to agglomerate, under MD, into the walls of the nanoporous architecture.[29] In particular, the amorphous nanoparticles are attractive to one another. Accordingly, the simulation cell size was reduced such that the nanoparticles are sufficiently close to one another that they agglomerate, under MD simulation, with their periodic neighbors in all three spatial directions. Specifically, a simulation cell size of 7.42 × 7.62 × 7.62 nm^3 was needed to effect this transformation. A more detailed explanation can be found in ref 19. The system was then crystallized by performing constant volume MD simulation at 2000 K for 10000 ps; simulated amorphization and crystallization has been described in more detail previously.[19] Finally, the structure was quenched to 0 K; MD simulation was performed for 100 ps at 0 K to yield a model for nanoporous $Li_{0.16}MnO_2$.

The mechanical properties of the mesoporous $Li_{0.16}MnO_2$ model structure were calculated by equilibrating the system to the target temperature by performing constant pressure MD

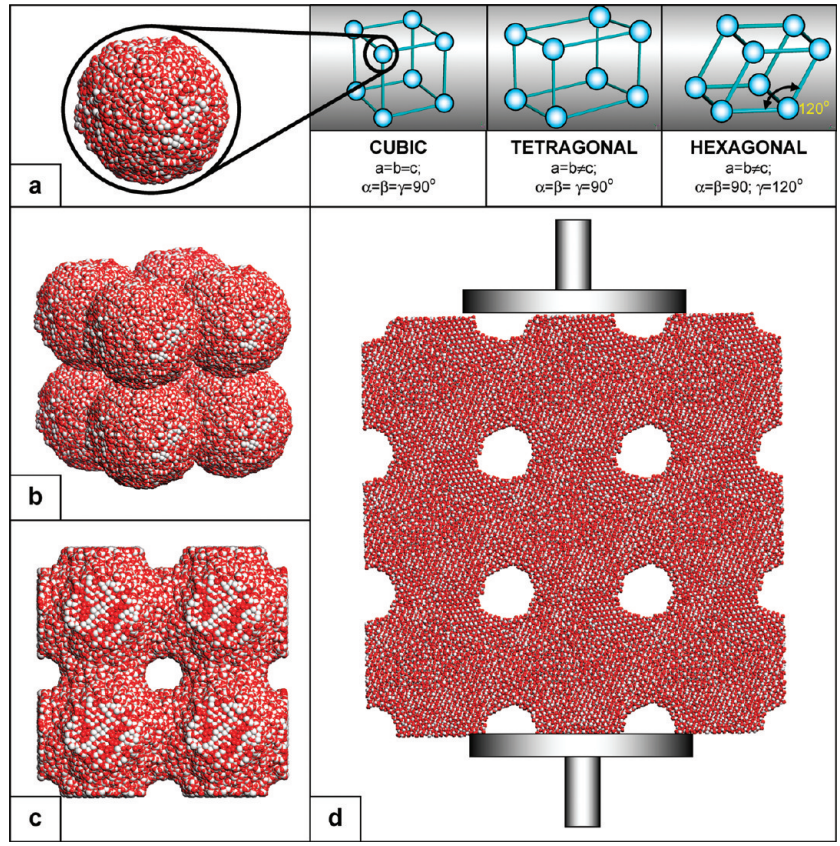

Figure 5. General strategy for generating a mesoporous structure and simulating its mechanical properties: (a) position amorphous nanosphere at crystallographic (basis) positions; (b) periodically repeat in three dimensions to facilitate particular space symmetry; (c) agglomerate neighboring amorphous nanospheres to formulate the walls of the framework architecture; (d) crystallize and simulate mechanical properties. Panels c and d show side views of a slice cut through the mesoporous material to show more clearly the channels. Mn is colored white, and oxygen is red; Li is not shown.

TABLE 1. Potential Parameters of the form $A\exp(-r/\rho) - Cr^{-6}$, Describing the Short-Range Potential Terms between the Component Ion Species of $LiMnO_2$; Terms Not Listed Are Set to Zero

interaction	A (Å)	ρ (Å)	C (eV. Å^6)	charge
$O^{2-}-O^{2-}$	11782.76	0.234	30.22	−1.1
Li^+-O^{2-}	30000.00	0.154	0.000	
Li^+-Li^+	270000.00	0.143	0.000	0.55
$Mn^{4+}-Mn^{4+}$	23530.50	0.156	16.00	2.2
$Mn^{4+}-O^{2-}$	15538.20	0.195	22.00	
$Mn^{3+}-Mn^{3+}$	33883.92	0.156	16.00	1.65
$Mn^{3+}-O^{2-}$	18645.84	0.195	22.00	
$Mn^{4+}-Mn^{3+}$	28707.21	0.156	16.00	

simulation at 300 K for 100 ps with 25 ps equilibration, prior to simulating tensile and compressive strain. Compression or tension was simulated by sequential scaling of the atom coordinates and performing constant volume MD simulation at 300 K; a strain rate of about 10^7 s^{-1} was achieved.

Acknowledgment. The authors thank the South African Research Chair Initiative of the Department of Science and Technology, National Research Foundation and the Centre for High performance Computing (CHCP) in South Africa, and R.R. Maphanga for simulating XRD patterns for our model Li_xMnO_2 nanostructures.

Supporting Information Available: Animations of the Molecular Dynamics simulations. (Video 1) Crystallization of mesoporous $Li_{0.16}MnO_2$. The animation shows a thin slice cut through the mesoporous MnO_2; sphere, stick, and polyhedral representations of the atom positions. MnO_6 species are represented by blue polyhedra, Mn^{4+} is dark blue, Mn^{3+} is light blue, O is red, and Li is yellow. (Video 2) Mesoporous $LiMnO_2$ under uniaxial tension. The animation shows a thin slice cut through the mesoporous $Li_{0.16}MnO_2$. Ball and stick model representation of the atom positions. Mn^{4+} is blue, Mn^{3+} is green, O is red, and Li is yellow. (Video 3) Mesoporous $Li_{0.16}MnO_2$ under hydrostatic compression revealing plastic deformation, which occurs along the grain-boundaries. The animation shows a thin slice cut through the mesoporous $Li_{0.16}MnO_2$ with a ball and stick model representation of the atom positions. Mn^{4+} is blue, Mn^{3+} is green, O is red, and Li is yellow. This material is available free of charge *via* the Internet at http://pubs.acs.org.

REFERENCES AND NOTES

1. Thomas, J. M.; Hernandez-Garrido, J. C.; Raja, R.; Bell, R. G. Nanoporous Oxidic Solids: The Confluence of Heterogeneous and Homogeneous Catalysis. *Phys. Chem. Chem. Phys.* **2009**, *11*, 2799–2825.
2. Lee, J.; Orilall, M. C.; Warren, S. C.; Kamperman, M.; Disalvo, F. J.; Wiesner, U. Direct Access to Thermally Stable and Highly Crystalline Mesoporous Transition-Metal Oxides with Uniform Pores. *Nat. Mater.* **2008**, *7*, 222–228.
3. Mobus, G.; Inkson, B. J. Nanoscale Tomography in Materials Science. *Mat.Today* **2007**, *10*, 18–25.
4. Ji, P. F.; Zhang, J. L.; Chen, F.; Anpo, M. Ordered Mesoporous CeO2 Synthesized by Nanocasting from Cubic Ia3d Mesoporous MCM-48 Silica: Formation, Characterization and Photocatalytic Activity. *J. Phys. Chem. C* **2008**, *112*, 17809–17813.
5. Jiao, F.; Bruce, P. G. Mesoporous Crystalline β-MnO_2 - A Reversible Positive Electrode for Rechargeable Lithium Batteries. *Adv. Mater.* **2007**, *19*, 657.
6. Dong, W. Y.; Sun, Y. J.; Lee, C. W.; Hua, W. M.; Lu, X. C.; Shi, Y. F.; Zhang, S. C.; Chen, J. M.; Zhao, D. Y. Controllable and Repeatable Synthesis of Thermally Stable Anatase Nanocrystal-Silica Composites with Highly Ordered Hexagonal Mesostructures. *J. Am. Chem. Soc.* **2007**, *129*, 13894–13904.
7. Wagner, T.; Waitz, T.; Roggenbuck, J.; Froba, M.; Kohl, C. D.; Tiemann, M. Ordered Mesoporous ZnO for Gas Sensing. *Thin Solid Films* **2007**, *515*, 8360–8363.
8. Yan, Q.; Shu-Juan, B.; Chang, M. L.; Xiao-Qiang, C.; Zhi-Song, L.; Jun, G. Nanostructured Polyaniline/Titanium Dioxide Composite Anode for Microbial Fuel Cells. *ACS Nano* **2008**, *2*, 113–119.
9. van Huis, M. A.; Kunneman, L. T.; Overgaag, K.; Xu, Q.; Pandraud, G.; Zandbergen, H. W.; Vanmaekelbergh, D. Low-Temperature Nanocrystal Unification through Rotations and Relaxations Probed by *in Situ* Transmission Electron Microscopy. *Nano Lett.* **2008**, *8*, 3959–3963.
10. Smarsly, B.; Antonietti, M. Block Copolymer Assemblies as Templates for the Generation of Mesoporous Inorganic Materials and Crystalline Films. *Eur. J. Inorg. Chem.* **2006**, *6*, 1111–1119.
11. Jiao, F.; Hill, A. H.; Harrison, A.; Berko, A.; Chadwick, A. V.; Bruce, P. G. Synthesis of Ordered Mesoporous NiO with Crystalline Walls and a Bimodal Pore Size Distribution DNA-Guided Crystallization of Colloidal Nanoparticles. *J. Am. Chem. Soc.* **2008**, *130*, 5262–5266.
12. Nykypanchuk, D.; Maye, M. M.; van der Lelie, D.; Gang, O. *Nature* **2008**, *451*, 549–552.
13. Suresh, S.; Li, J. Deformation of the Ultra Strong. *Nature* **2008**, *456*, 716–717.
14. Uchic, M. D.; Holzer, L.; Inkson, B. J.; Principe, E. L.; Munroe, P. Three-dimensional Microstructural Characterization Using Focused Ion Beam Tomography. *Mater. Res. Bull.* **2007**, *32*, 408–416.
15. Suresh, S. Li, Materials Science Deformation of the Ultra-Strong. *Nature* **2008**, *456*, 716–717.
16. Moebus, G.; Inkson, B. J. Nanoscale Tomography in Materials Science. *Mater. Today* **2007**, *10*, 18–25.
17. Lockwood, A. J.; Inkson, B. J. *In Situ* TEM Nanoindentation and Deformation of Si-Nanoparticle Clusters. *J. Phys. D: Appl. Phys.* **2009**, *42*, 035410.
18. Wolf, D.; Yamakov, V.; Phillpot, S. R.; Mukherjee, A.; Gleiter, H. Deformation of Nanocrystalline Materials by Molecular-Dynamics Simulation: Relationship to Experiments. *Acta Mater.* **2005**, *53*, 1–40.
19. Sayle, D. C.; Seal, S.; Wang, Z.; Mangili, B. C.; Price, D. W.; Karakoti, A. S.; Kuchibhatla, S. V. T. N.; Hao, Q.; Mobus, G.; Xu, X.; Sayle, T. X. T. Mapping Nanostructure: A Systematic Enumeration of Nanomaterials by Assembling Nanobuilding Blocks at Crystallographic Positions. *Acs Nano* **2008**, *2*, 1237–1251.
20. Yamakov, V.; Wolf, D.; Phillpot, S. R.; Mukherjee, A. K.; Gleiter, H. Deformation-Mechanism Map for Nanocrystalline Metals by Molecular-Dynamics Simulation. *Nat. Mater.* **2004**, *3*, 43–47.
21. Xiong, L. M.; Chen, Y. P.; Lee, J. D. Atomistic Measure of the Strength of MgO Nanorods. *Theor. Appl. Fract. Mech.* **2006**, *46*, 202–208.
22. Luo, J. Y.; Zhang, J. J.; Xia, Y. Y. Highly Electrochemical Reaction of Lithium in the Ordered Mesoporosus β-MnO_2. *Chem. Mater.* **2006**, *18*, 5618–5623.
23. Bruce, P. G.; Bruno Scrosati, B.; Tarascon, J.-M. Nanomaterials for Rechargeable Lithium Batteries. *Angew. Chem., Int. Ed.* **2008**, *47*, 2930–2946.
24. Lu, D.; Katou, T.; Uchida, M.; Kondo, J. N.; Domen, K. *In Situ* TEM Observation of Crystallization of Amorphous Ordered Mesoporous Nb−Ta and Mg−Ta Mixed Oxides. *Chem. Mater.* **2005**, *17*, 632–637.
25. Piana, S.; Reyhani, M.; Gale, J. D. Simulating Micrometre-Scale Crystal Growth from Solution. *Nature* **2005**, *438*, 70–73.
26. Chabre, Y.; Pannetier, J. Structural and Electrochemical Properties of the Proton γ-MnO_2 System. *Prog. Solid State Chem.* **1995**, *23*, 1–130.
27. Balachandran, D.; Morgan, D.; Ceder, G.; van de Walle, A. First-Principles Study of the Structure of Stoichiometric and Mn-Deficient MnO_2. *J. Solid State Chem.* **2003**, *173*, 262–75.
28. Sayle, T. X. T.; Catlow, C. R. A.; Maphanga, R. R.; Ngoepe, P. E.; Sayle, D. C. Generating MnO_2 Nanoparticles Using Simulated Amorphization and Recrystallization. *J. Am. Chem. Soc.* **2005**, *127*, 12828–12837.
29. Sayle, T. X. T.; Maphanga, R. R.; Ngoepe, P. E.; Sayle, D. C. Predicting the Electrochemical Properties of MnO_2 Nanomaterials Used in Rechargeable Li Batteries: Simulating Nanostructure at the Atomistic Level. *J. Am. Chem. Soc.* **2009**, *131*, 6161–6173.
30. Smith, W.; Forester, T. R. *DL_POLY*; Council for the Central Laboratory of the Research Councils, Daresbury Laboratory: Daresbury, Warrington, U.K., 1996; www.cse.clrc.ac.uk/msi/software/DL_POLY/.
31. Humphrey, W.; Dalke, A.; Schulten, K. VMD—Visual Molecular Dynamics. *J. Mol. Graphics* **1996**, *14*, 33–38, www.ks.uiuc.edu/Research/vmd/.